Tertiary Structure of Endothelin-1 in Water by ^{1}H NMR and Molecular Dynamics Studies

Enzio Ragg,[a] Rosanna Mondelli,*[,a] Sergio Penco,[b] Giorgio Bolis,[b] Luca Baumer[b] and Alberto Guaragna[b]

[a] *Università di Milano, Dipartimento di Scienze Molecolari Agroalimentari, Via Celoria 2, 20133 Milano, Italy*
[b] *Pharmacia, Ricerca e Sviluppo, Via Giovanni XXIII 23, 20014 Nerviano, Italy*

The 3D structure in pure water of endothelin-**1**, a recently discovered potent vasoconstrictor peptide, has been determined at different pH and temperatures, using two-dimensional ^{1}H NMR spectroscopy and constrained molecular dynamics (MD). 170 Inter- and intra-residue NOE interactions were quantified as volume integrals and translated into distances. All the coupling constants between the amidic and the α-protons have been measured and several dihedral angles, thus obtained, have been used as constraints for the MD. Some stereospecific assignments have also been performed. A family of eleven structures, satisfying the distance constraints to within 0.3 Å, was obtained and showed that the C-terminal, determinant for the binding with the receptor, has a well defined conformation. The correlation time measurements gave an average molecular volume consistent with monomeric species. The tertiary structure at neutral pH is that of a compact molecule, in which the C-terminal of the peptide folds back toward the α-helical segment (residues 9–16), in close proximity to the pro-*R* methyl group of Val^{12}, as defined by important NOEs involving residues 17–21 and the α-helical core residues 9–14. The results are in agreement with the deuterium exchange experiments, which confirm the existence of a hydrophobic region also at the site of the C-terminal residues 19–21.

Since the first report of Yanagisawa *et al.*[1] there has been a surge of investigation into the endothelin family of peptides,[2–12] because of their extremely potent vasoconstrictive activity and other interesting biological properties.[11] Now there are many indications that endothelins are involved as local factors in the regulation of the cardiovascular system, and evidence to suggest that endothelin-**1** (**ET-1**) may be implicated in the pathophysiology of a number of vascular conditions.[12] Although the effects of exogenous endothelin have been widely studied, the mechanisms of action of endogenous endothelin are still unclear.[11,12] **ET-1** is a 21-amino acid peptide having four cysteine residues at position 1,3,11 and 15 connected by two disulfide bridges 1–15 and 3–11. A similar bicyclic structure has been shown to be present in apamin,[13] a neurotoxic peptide component of honeybee venom, and in sarafotoxins found in the venom of Israeli asp. The similar activities of endothelins and sarafotoxins have suggested a common evolutionary origin.[14]

The correlation between structure and activity is one of the most urgent reasons for the characterization of these peptides. The structure in aqueous solution might give insight into the conformation in biological conditions, as well as suggesting working hypotheses for possible interaction with the receptor. This information could also be relevant for designing synthetic receptor antagonists.[15]

Up to now the reported structural results have been obtained only from experimental data in Me_2SO solution, or in media containing organic solvents.[2–8] The studies on **ET-1** tend to concur in that the first part of the molecule is characterised by a helix conformation from residues 6–11,[4] 11– or 9–15,[2a] 9–16.[3,5–8] On the other hand the four proposed structures in Me_2SO[2–4] differ significantly with each other; in addition, the C-terminal tail, so important for both binding and receptor activation,[16] in all the studies except for one paper reporting experiments in Me_2SO.[2a] is undefined or said to be flexible, since no NOE interactions have been observed between the tail and the rest of the molecule.

Thus the tertiary structure of **ET-1** is still unclear, and no studies in water, the only solvent with direct relevance to biology, up to now have been reported. To better characterise the conformation of endothelin and the behaviour of the important C-terminal tail, we now report the tertiary structure of **ET-1** in pure water by extensive use of one- and two-dimensional ^{1}H NMR experiments at different pHs and concentrations and by using constrained molecular dynamics calculations.

Experimental

ET-1 (Novabiochem) was used without further purification. The absence of traces of Hg was ascertained by atomic absorption spectroscopy as some authors[4] have advanced the hypothesis that some samples, for instance those used for the Me_2SO study,[2a] might contain impurities of Hg depending on the synthetic pathway.

NMR Spectroscopy.—^{1}H NMR experiments were performed at 600.13 MHz on a Bruker AMX-600 spectrometer both in H_2O–D_2O (90:10) and in D_2O 99.9% at pH 7.0, 6.3, 3.5 and 2.0. After dissolving **ET-1** (1 mg) in H_2O or D_2O (0.5 cm^3) at 5 °C under nitrogen, a pH of 3.5 was measured and in these conditions 1D and 2D NMR spectra were acquired; the signals were sharp and the solution was clear and stable for at least 12 h. The pH was varied by adding vapours of NH_3 or of trifluoroacetic acid. At pH 7.0 and 6.3 the solutions are stable

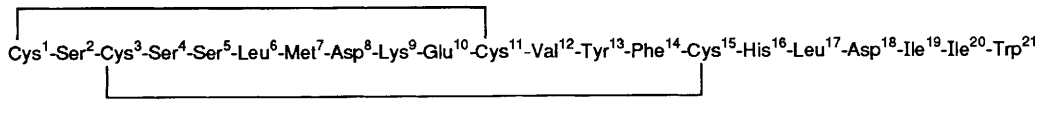

ET-1

and 2D NMR spectra were measured at 5, 12 and 23 °C, with an average concentration of 3 mg cm^{-3}. 1D NMR spectra were measured in H_2O (pH 6.3) throughout the temperature range 5–25 °C and with increasing dilution from 5 to 0.2 mg cm^{-3}, in order to observe the shift variation and exclude the formation of micelles. The shift variation of NH signals with temperature and pH was studied at pH 6.3 (temperature range 5–25 °C) and at 5 °C (pH 3.5 and 6.3) respectively. The water suppression was obtained during the preparatory delay, 1.5 s for either 1D and 2D experiments; for 1D experiments at pH 6.0 and 14 °C we also used the binomial 1331 pulse sequence.[17] Chemical shifts (Table 1) are in δ values from external 3-(trimethylsilyl)-propane-1-sulfonic acid, sodium salt hydrate in D_2O (DSS) and are accurate within ±0.005 ppm. Coupling constants were measured from 1D spectra, but $J_{\alpha,\beta}$ were also obtained from the αβ cross-peaks in DQF–COSY 2D spectra.[18] Accuracy is ±0.05 Hz unless specified in Table 2. $J_{\alpha,\beta}$ were measured in D_2O at 23 °C, pH 6.0 and 7.0. $J_{\alpha,NH}$ were obtained from H_2O solution at 23 and 14 °C, pH 6.0 and 2.0 by using presaturation and the 1331 pulse sequence[17] for the water suppression (see Fig. 1). Amide NH exchange experiments were performed by acquiring 1D serial spectra at 5 min to 6 h after **ET-1** was dissolved in D_2O at pH 3.5; the temperature was set at 5 °C for 3 h, then at 12 °C for the remaining 3 h. The sample was then lyophilised and dissolved in H_2O, observing the NH re-appearance with the same temperature and time intervals.

The signals of all protons were assigned by 2D TOCSY (spin lock of 60 ms, no TRIM pulse), ROESY and NOESY experiments.[18] In each 2D experiment, 512 × 1 K spectra were acquired in TPPI mode and processed with zero filling to 2 K × 2 K points and weighted with a squared sinebell function. Cross-peaks in NOESY spectra were integrated after baseline correction with a 5th order polynomial using the standard Bruker Uxnmr software. The volumes were translated in interatomic distances using the 'two-spin' approximation eqn. (1):

$$r_{ij} = r_{ref}(V_{ref}/V_{ij})^{1/6} \quad (1)$$

V_{ref} and r_{ref} were taken from averages of known distances (vicinal protons with measured coupling constant, like $d_{\alpha\beta}$ of Val^{12} and $d_{\alpha NH}$). With this reference value, the measured average d_{NHNH} distance in the region between residues 7 and 15 of endothelin was found to be 2.7 Å, consistent with an average proton–proton distance within an α-helical region. Distances involving methyl groups were calculated using as reference volume the cross-peak intensity of Val^{12}Me–Val^{12}βH interaction. All methyls were assumed to have the same correlation time. The linearity of the NOE build-up with mixing time was checked by calculating NOESY intensities from the relaxation matrix of the complete proton spin system, using model geometries and a correlation time of 2 ns (as calculated from known distances, see later). It was found that for intra-residue distances, $d_{\alpha\beta}$ and $d_{\alpha NH}$, and for $d_{NH,NH}(i, i + 1)$ the approximation is valid up to 400 ms. Longer distances were more affected by spin diffusion, but because some of the crucial NOEs (*i.e.* those involving long-range interactions) were not measurable at a 150 ms mixing time, they were quantified at 300 ms and translated into distance constraints with weaker force constants.

Computational Methods.—The derivation of the structures was performed using Biosym software (Discover, Insight, NMRchitet) on the Silicon Graphics 4D320VGX and 4D35GTX computers. The methodology for the derivation of structures was a Simulated Annealing (SA) procedure, applied about 200 times and consisting of the following steps. A random distribution in space of the atoms constituting the **ET-1** molecule were generated at first and an initial constrained minimization was performed with all the terms of the potential function scaled to zero, except for the terms of the NOE constraints. Then a constrained molecular dynamics (MD) simulation at 1000 K were executed for 25 ps. During this simulation the force constants for all the terms of the potential energy function were increased gradually until they reached their normal scale factor of 1. The successive steps of constrained MD simulation were performed for 10 ps and with temperature gradually decreasing from 1000 to 300 K. Finally, a constrained minimization followed the MD simulation to bring each structure to a local minimum. The force constants for the NOE constraints were set to a value of 209.20 KJ $Å^{-2}$ whenever the atoms involved were intraresidue or in nearest neighbour residues, while for all the other pairs of atoms a value of 125.52 KJ $Å^{-2}$ was chosen. The structures were then analysed and, after selection of the best ones, a further constrained dynamics and minimization were performed to refine the agreement with the experimental data.

Results and Discussion

ET-1 in water displays well-resolved resonances at both acidic and neutral pHs. All NOEs at 600 MHz are negative and with a good signal-to-noise ratio. A correlation time of about 2 ns was obtained by using NOE interactions between protons at known distance, *i.e.* geminal protons and αH–NH pairs, where the coupling constants allowed to define the dihedral angles. The correlation time value obtained using the Debye–Stokes–Einstein equation[19] gave the average molecular volume (800×10^{-23} cm^3), which is consistent with solvated monomeric species. As circular dichroism measurements in water[10] suggested the formation of micelles, we also performed experiments at variable concentrations at pH 6.3 from 6 down to 0.2 mg cm^{-3} and we found no shift variation for the non-exchangeable aromatic protons. This result, together with the correlation time value, indicates that in our experimental conditions **ET-1** is essentially monomeric. On the other hand, we observed the slow formation of a gel when the temperature rises above 5 °C at pH 2.0–3.5. In these conditions the NMR resolution drops down, and no signal is detectable.

Sequential Resonance Assignments.—The signals were assigned using a series of NOESY, COSY and TOCSY spectra following the strategy for protein structure.[18] As the primary structure was known,[1] the procedure was established relatively easily. All ambiguities were resolved by acquiring NOESY spectra at different temperatures.

The spin systems of the non labile protons in individual amino acid residues were identified in D_2O solution using, as far as possible, through-bond H–H connectivities by TOCSY experiments. The aromatic protons of Tyr, Phe, His and Trp were assigned from 1D spectra by the chemical shift values and the multiplicity of the signals, *i.e.* AA'BB' spin system for Tyr, AA'BB'C for Phe, ABCD for Trp. The scalar interactions, detected by COSY spectra, allowed the assignments within each spin system. The aromatic protons gave NOE connectivities to the corresponding βH and/or αH resonances which were thus identified. From spectra in H_2O solution, the spin system of the individual amino acid residues were completed by identification of the corresponding amidic NH protons. Sequentially neighbouring amino acid spin systems were then assigned from observation of the $(i,i + 1)$ NOE connectivities d_{NHNH}, $d_{\alpha NH}$ and $d_{\beta NH}$.* The sequential NOE cross-peaks were observed for

* $d_{NHNH}(i, i + 1)$ represents the sequential NOE connectivity between the NH protons of two neighbouring residues; $d_{\alpha,NH}$ and $d_{\beta,NH}$ the connectivities of αH and βH respectively to the NH of the neighbouring residue.

Table 1 ^{1}H Chemical shift assignments for endothelin-**1** in water[a]

	pH 3.5, 5 °C					pH 6.0, 5 °C					pH 6.0, 23 °C				
Residue	NH	αH	βH	β'H	Others	NH	αH	βH	β'H	Others[b]	NH	αH	βH	β'H	Others[b]
Cys[1]	*c*	4.24	3.17	3.17		*c*	4.25	3.21	3.21		*c*	4.26	3.27	3.27	
Ser[2]	8.96	4.62	3.71	3.71		8.97	4.69	3.77	3.77		8.90[r]	4.76	3.84	3.83	
Cys[3]	8.32	*d*	3.07	2.44		8.42	*d*	3.16	2.44		8.27	5.00	3.23[e]	2.54[f]	
Ser[4]	8.88	4.17	3.85	3.78		9.12	4.20	3.89	3.85		9.07[r]	4.28	3.96	3.92	
Ser[5]	7.78	4.46	3.83	3.59		7.86	4.56	3.88	3.72		7.83[r]	4.60	3.93	3.77	
Leu[6]	8.55	4.04	1.46	1.37	γ 1.54, δ 0.78,[g] 0.70[g]	8.67	4.12	1.60	1.53	1.60, 0.83, 0.76	8.57	4.19	1.65	1.62	1.65, 0.90, 0.81
Met[7]	7.96	4.35	2.07	1.78	γ 2.52, 2.36, 1.97[g]	8.07	4.42	2.13	1.82	2.59, 2.41, 2.00	8.05	4.47	2.19[e]	1.89[f]	2.64, 2.48, 2.02
Asp[8]	7.41	4.35	3.13	2.75		7.34	4.59	3.11	2.56		7.40	4.63	3.12[f]	2.62[e]	
Lys[9]	8.19	3.77	1.70	1.67	γ 1.37, 1.20, δ 1.50, ε 2.80, 7.43[t]	8.21	3.81	1.77	1.70	1.41, 1.18, 1.54, 2.87	8.19	3.89	1.82[e]	1.77[f]	1.47, 1.32, 1.61, 2.90
Glu[10]	8.39	4.06	1.98	1.98	γ 2.35	8.39	4.09	2.04	2.04	2.27	8.37	4.15	2.11	2.11	
Cys[11]	7.49	4.18	3.08	3.00		7.71	4.30	3.11	3.04		7.75	4.35	3.20[e]	3.13[f]	
Val[12]	8.09	3.39	1.93		γ 0.88,[g] 0.75[g]	8.32	3.45	2.00		0.97, 0.81	8.24	3.52	2.06		1.01,[e] 0.86[f]
Tyr[13]	7.80	4.18	2.93	2.91	6.78,[h] 6.61[i]	7.91	4.29	3.01	2.99	6.93, 6.71	7.86	4.35	3.04	3.05	6.98, 6.78
Phe[14]	8.22	4.04	3.10	3.08	7.18,[l] 7.25[i]	8.23	4.12	3.18	3.17	7.29, 7.34	8.19	4.22	3.24[e]	3.25[f]	7.35, 7.41
Cys[15]	8.54	4.46	3.14	2.82		8.60	4.53	3.19	2.79		8.56	4.60	3.24	2.87	
His[16]	7.81	4.38	3.15	3.16	8.35,[m] 7.07[n]	7.88	4.43	3.25	3.23	8.29, 7.08[s]	7.84	4.48	3.32	3.31	8.33, 7.14
Leu[17]	7.80	4.11	1.51	1.47	γ 1.37, δ 0.67[g]	8.08	4.28	1.56	1.51	1.43, 0.79	8.05	4.34	1.62	1.57	1.50, 0.85
Asp[18]	8.28	4.48	2.76	2.61		8.46	4.45	2.53	2.50		8.42	4.52	2.59	2.56	
Ile[19]	7.74	3.90	1.49		γ 1.17, 0.85, γ 0.31,[g] δ 0.59[g]	7.77	3.91	1.54		1.24, 0.89, 0.30, 0.67	7.70	4.01	1.63		1.30, 0.98, 0.45, 0.73
Ile[20]	8.02	4.01	1.65		γ 1.26, 0.98, γ, δ 0.70,[g] 0.68[g]	8.07	4.08	1.73		1.30, 1.04, 0.75, 0.76	7.91	4.15	1.79		1.34, 1.08, 0.81, 0.81
Trp[21]	8.12	3.90	3.20	3.09	7.08,[m] 7.48,[n] 6.98,[o] 7.28,[p], 9.97[q]	7.73	4.42	3.24	3.05	7.15, 7.62, 7.08,[s] 7.36, 10.04	7.63	4.50	3.29[e]	3.13[f]	7.20, 7.67, 7.14, 7.42, 10.00

[a] Measured in ppm (δ) from external DSS reference. [b] For the assignments see the 6th column. [c] Undetected because of fast exchange. [d] Overlapped by water signal. [e,f] Stereospecific assignment, pro-*S* and pro-*R* respectively. [g] Me. [h] 2,6-H. [i] 2,4,6-H. [l] 2,4,6-H. [m] 2-H. [n] 4-H. [o] 5,6-H (centre of the multiplet). [p] 7-H. [q] Indolic NH. [r] Detected at 14 °C and by using the binomial 1–3–3–1 pulse sequence for water suppression.[17] [s] The signals of His[16] (4-H) and Trp[21] (5,6-H) are well separated at pH 7.1, 5 °C (δ 7.03 and 7.07 respectively) thus allowing the assignment of the NOE interactions involving the two residues. [t] $Lys^9NH_3^+$.

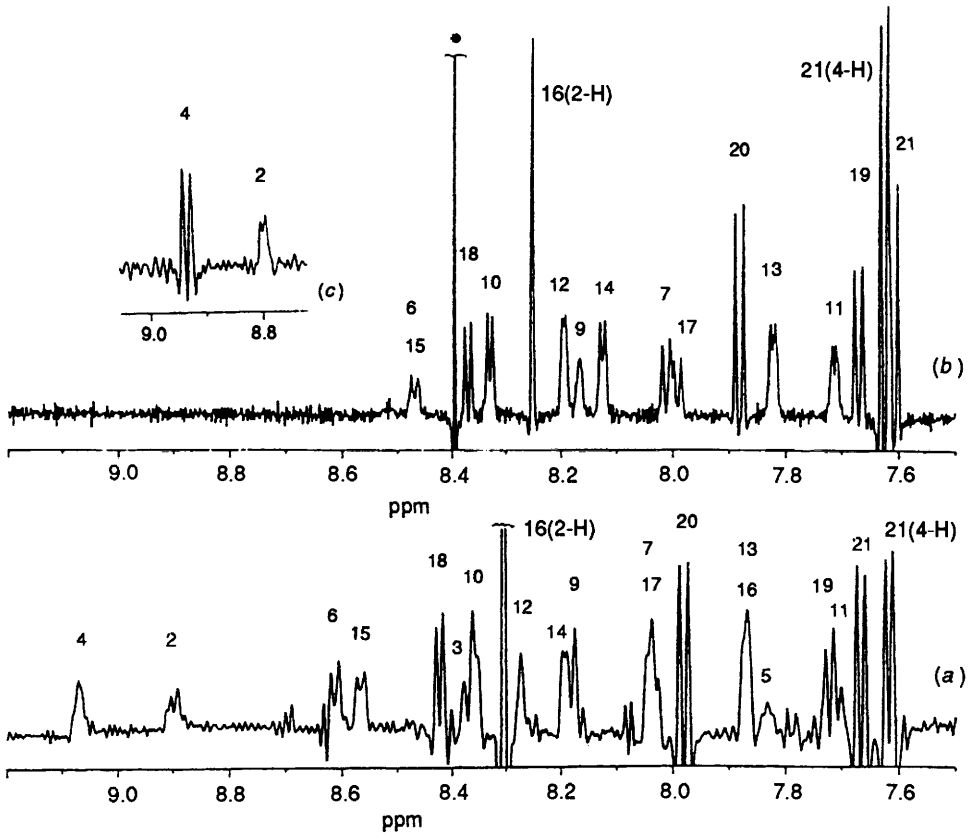

Fig. 1 NH region of ^{1}H NMR spectra of **ET-1** in water 90%; (*a*) at pH 6.3, 14 °C and with 1331 pulse sequence for water suppression; (*b*) at pH 6.3, 23 °C and with presaturation of water signal; (*c*) at pH 2.0, 20 °C. The numbers on the signals indicate the amino acid residue, the asterisk an electronic spike.

nearly all residues; the NH–NH interactions were missing, for Cys^3–Ser^4, Ser^5–Leu^6, Asp^8–Lys^9 and His^{16}–Leu^{17}, but we could find all the βH–NH interactions. Of the αH–NH interactions, only Cys^3–Ser^4 was missing, whereas His^{16}–Leu^{17} might be overlapped by other signals, but their assignments were straightforward. Actually the connectivities involving the three serines and the cysteines at the 1 and 3 positions were a little difficult to define, because the NH protons of these residues are in fast exchange at temperatures higher than 5 °C. The following procedure was used: at 5 °C, starting from the unambiguously assigned Ser^5, we identified Ser^4 by their NH–NH cross peak. Thus the remaining serine must be Ser^2. As we observed strong NH–NH and βH–NH NOESY cross-peaks between Ser^2 and a cysteine residue, this cysteine must be Cys^3. On the other hand the amidic NH proton of Cys^3 and Ser^2 could not be interchanged because the β protons of cysteines and serines, identified by TOCSY correlation, have unambiguously different chemical shifts. The assignment at 23 °C were thus completed by using the results at 5 °C and the 1D spectra with the 1331 pulse sequence (see Fig. 1). The complete resonance assignments are reported in Table 1.

Stereospecific Assignments.—Pro-*R*/*S* assignments were performed for the methyl groups of Val^{12} and for the β protons of the three cysteines, of Met^7, Asp^8, Lys^9 and Trp^{21} (Table 1). Following the procedure of Wagner and Wüthrich,[20] we used the $J_{\alpha\beta}$ coupling constants values and the intraresidue βH–NH NOE interactions. In the case of Cys^{15} and Trp^{21} the pro-*R*/*S* assignment was only tentative, due to partial signals overlap, and they were thus not considered as constraints in the calculations.

NOE, Coupling Constants and Deuterium Exchange Results.—About 250 inter- and intra-residue NOE correlations were analysed for each spectrum, obtained in different condition of pH and temperature. Fig. 2 show segments of NOESY experiments.

At 23 °C the NH signals of the three serines and of Cys^3 are in a relative fast exchange regime, as appears from the 1D spectrum reported in Fig. 1. Consequently, some of the cross-peaks related to Cys^3 and to the serines were missing at room temperature [see Fig. 2(*a*)], whereas at 5 °C all the amidic NH protons were visible at either pH 3.5 [Fig. 2(*b*)] or 6.5. In the 1D spectrum reported in Fig. 1(*b*) the exchange between NH protons and water was decreased by acquiring without the water presaturation procedure. We selected the high quality spectra of Fig. 1 in order to measure the coupling constants $J_{\alpha,NH}$, which however showed the same values until 10 °C; at lower temperature the resolution is too poor for *J*s measurements. At acidic pH, as said before, it is difficult to work at temperatures higher than 5 °C; experiments performed at 20 °C gave some *J*s values, *i.e.* Ser^2 9.0, Ser^4 6.5, Met^7 9.0, His^{16} 7.5, Leu^{17} 7.5, Ile^{19} 8.5 and Ile^{20} 8.0 Hz.

An inspection of Table 2 shows that the values of $J_{\alpha,NH}$ are lower than 6.0 Hz for the fragment from Lys^9 to Phe^{14}, whereas they range between 7.0 and 9.0 Hz for the N-terminal and the C-terminal parts of the molecule (residues 2–8 and 16–21 respectively). This suggests[18] that the middle segment (residues 9–14) is conformed in a helix secondary structure.

Evidence for the prevalence of an α-helix must be revealed by the observation of strong medium range (*i*, i + 3) αH–βH and αH–NH NOE interactions, which are absent in all the other non-helical conformations. The αH–NH (*i*, *i* + 3) NOEs are common to α-helix and 3_{10}-helix, which on the other hand could be distinguished by the presence of (*i*, *i* + 4) or (*i*, *i* + 2) αH–NH NOEs respectively.[18] We found strong αH–βH and αH–NH interactions between the pairs of residues 9–12, 10–13 and

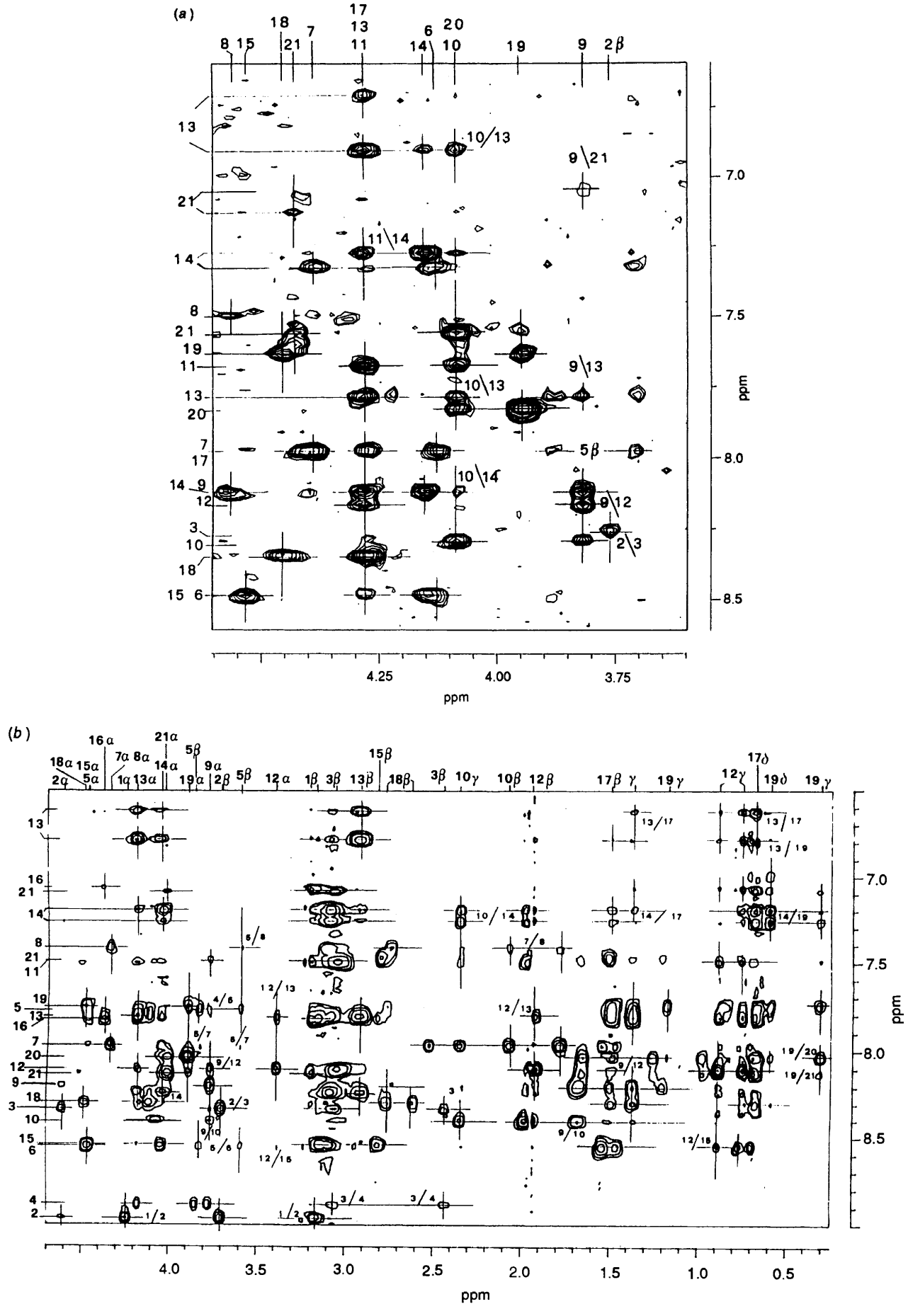

Fig. 2 NOESY spectra of **ET-1** in water 90% (t_{mix} 300 ms) showing the NOE interactions of amidic and aromatic protons. The numbers on the left border indicate the NH and the aromatic proton resonances for some residues; (*a*) pH 6.3 and 23 °C, NH/α region; (*b*) pH 3.5 and 5 °C, NH/α–δ region.

Table 2 H,H coupling constant values (Hz) for endothelin[a]

Residue	$J_{\alpha,NH}$	$J_{\alpha,\beta}$	$J_{\alpha,\beta'}$	Residue	$J_{\alpha,NH}$	$J_{\alpha,\beta}$	$J_{\alpha,\beta'}$
Ser^2	9.0[b]	5.2	5.7	Val^{12}	4.5	8.7[e]	
Cys^3	9.7	4.0	10.5	Tyr^{13}	5.5	16.5[f]	
Ser^4	7.0[d]	5.5	4.5	Phe^{14}	6.0	16.2[f]	
Ser^5	*c*	5.7	7.1	Cys^{15}	7.5	4.5	11.2
Leu^6	8.25[b]	(4.5)	(10.7)	His^{16}	7.5[d]	*c*	*c*
Met^7	8.5	4.0	11.0	Leu^{17}	7.0	(5.0)	(6.0)[e]
Asp^8	6.8	10.2	5.3	Asp^{18}	7.5	(6.3)	(7.3)[e]
Lys^9	⩽4.0	9.8[e]	5.2[e]	Ile^{19}	8.5	8.3	
Glu^{10}	5.5	15.7[f]		Ile^{20}	9.0	8.5	
Cys^{11}	5.0	5.3[e]	10.5[e]	Trp^{21}	8.0	4.7	8.3

[a] Water solution, pH 6.0, 23 °C, estimated accuracy ±0.1 Hz, unless specified. The values in parenthesis may be interchanged. With β and β′ are given the proton in β position at low and high field respectively. For Cys^1 the analysis was impossible due to the absence of the amidic NH and the degeneracy of β and β′ protons. [b] Obtained at 14 °C. [c] Signal too broad or hidden. [d] Obtained at pH 2.0 and 20 °C. [e] Accuracy ±0.2 Hz. [f] The sum of the two coupling constants only was detected, because of the degeneracy of β and β′ protons.

12–15 (Fig. 2 and Table 3), corresponding to $d_{\alpha,\beta}$ (i, i + 3) distances of 2.54, 3.27, 3.39 Å and to $d_{\alpha,NH}$ distances of 2.99, 3.14 and 3.99 Å. In addition NOE cross-peaks between 11–14 and 13–16 were also observed but were not quantitated as volume integrals because partially overlapped by other signals. This finding proves the helix secondary structure for the segment from Lys^9 to Cys^{15}. That the helix is an α-helix follows from the absence of any (i, i + 2) αH–NH interactions, characteristic for a 3_{10}-helix. On the other hand, the αH–NH (i, i + 4) NOEs, suggested[18] as diagnostic for the α-helix, are in general very weak and might be confused with secondary NOE peaks. We found such interactions between residues 9–13 and 10–14, whereas those involving the pairs 11–15 and 12–16 were obscured by other signals; thus we did not include them in the constraints list. The α-helix structure appeared to be quite stable and independent from the pH and temperature (range 5–25 °C), as partially shown by comparing Figs. 2(*a*) and 2(*b*); irregular conformation at the position of Cys^{15} was suggested by the 7.5 Hz value of $J_{\alpha,NH}$ for Cys^{15} and then confirmed by the MD calculation (see later).

Important long-range interactions between the C-terminal part of the molecule (residues 17–21) and the core (residues 9–15) were detected (see Table 3). In particular Lys^9αH and the pro-*R* methyl group of Val^{12} have contacts with the aromatic protons of Trp^{21}; Val^{12}αH also shows an intense cross-peak with Leu^{17}βH. These results are strengthened by the interactions of the aromatic rings of Tyr^{13} and Phe^{14} with the δ methyl protons of Ile^{19} and Leu^{17} (Fig. 2). Although many of these interactions were observed in the side-chains, two significant long-range contacts, *i.e.* 9–21 and 12–17, involve the αH backbone protons of Lys^9 and Val^{12}. Moreover, we must remark that the most important NOE interactions were observed at low (5 °C) and high (23 °C) temperatures and at either acidic or neutral pH. The only exception concerns Lys^9, which did not present the interaction with Trp^{21} at acidic pH; in addition the cross-peaks of Val^{12} with Trp^{21} are very weak.

The interpretation of all these data indicates that the C-terminal part of **ET-1** (residues 17–21) preferentially assumes conformations folded toward the core of the molecule (residues 9–15); this does not exclude the presence of other conformers, which however must be less populated. The fact that the whole **ET-1** assumes an ordered structure (intended as a family of similar structures) in water solution, follows also from a significant spread in the chemical shifts; the deviation from

Table 3 Summary of medium and long-range NOE interactions[a]

Residue	Proton(s)[b]	Residue	Proton(s)[b]
Ser^2	αH	Leu^6	Me
Ser^2	ββ′H[c]	Leu^6	Me
Cys^3	β′H(pro-*R*)	Cys^{11}	β′H(pro-*R*)
Cys^3	βH(pro-**S**)	Val^{12}	Me(pro-*S*)
Ser^5	αH	Met^7	NH
Ser^5	β′H[d]	Asp^8	NH
Ser^5	β′H[d]	Asp^8	β′H(pro-*S*)
Ser^5	β′H	Cys^{11}	β′H(pro-*R*)
Leu^6	αH	Val^{12}	Me(pro-*S*)
Lys^9	αH	Val^{12}	NH
Lys^9	αH	Val^{12}	βH
Lys^9	αH	Val^{12}	Me(pro-*S*)
Lys^9	αH	Tyr^{13}	NH
Lys^9	αH	Trp^{21}	5, 6-H[e]
Glu^{10}	NH	Val^{12}	NH
Glu^{10}	αH	Tyr^{13}	NH
Glu^{10}	αH	Tyr^{13}	ββ′H
Glu^{10}	αH	Tyr^{13}	2, 6-H
Glu^{10}	αH	Phe^{14}	NH
Glu^{10}	ββ′H	Phe^{14}	2, 4, 6-H
Cys^{11}	β′H(pro-*R*)	Val^{12}	Me(pro-*S*)
Cys^{11}	NH	Val^{12}	Me(pro-*S*)
Cys^{11}	NH	Tyr^{13}	NH
Cys^{11}	αH	Phe^{14}	2, 4, 6-H
Val^{12}	αH	Cys^{15}	NH
Val^{12}	αH	Cys^{15}	βH
Val^{12}	αH	Cys^{15}	β′H
Val^{12}	αH	Leu^{17}	βH
Val^{12}	αH	Leu^{17}	γH
Val^{12}	Me(pro-*R*)	Trp^{21}	5, 6-H[e]
Tyr^{13}	2, 3, 5, 6-H	Phe^{14}	(2–6)-H
Tyr^{13}	2, 6-H[f]	Leu^{17}	ββ′H
Tyr^{13}	2, 6-H[f]	Leu^{17}	γH
Tyr^{13}	3, 5-H	Ile^{19}	δMe
Phe^{14}	2, 4, 6-H[g]	Leu^{17}	ββ′H
Phe^{14}	2, 4, 6-H[g]	Leu^{17}	Me
Phe^{14}	3, 5-H	Ile^{19}	δMe
Cys^{15}	βH	Leu^{17}	Me
Cys^{15}	β′H	Leu^{17}	Me
Cys^{15}	βH	Leu^{17}	γH
Cys^{15}	β′H	Leu^{17}	γH
His^{16}	2-H	Leu^{17}	Me
His^{16}	4-H	Leu^{17}	Me
Ile^{19}	γMe	Ile^{20}	NH
Ile^{19}	αH	Trp^{21}	NH
Ile^{19}	γMe	Trp^{21}	NH
Ile^{19}	γMe	Trp^{21}	2-H
Ile^{19}	δMe	Trp^{21}	5, 6-H
Ile^{19}	δMe	Trp^{21}	7-H
Ile^{20}	γ, δMe[h]	Trp^{21}	NH
Ile^{20}	γ, δMe[h]	Trp^{21}	5, 6-H

[a] The (i, i + 1) αH–βH, αH–βNH, βH–NH, NH–NH and the intra-residue NOE interactions are not included in this list. [b] Nuclei involved in the NOE interaction. [c] β and β′H stand for lowfield and upfield proton respectively. [d] From MD results, the pro-*R* proton of Ser^5 is the nucleus involved in the NOE interactions. [e] At pH 6.0 only. [f] All the aromatic protons of Tyr^{13} present NOE cross-peaks; it was not possible to distinguish the primary from the secondary NOE. From MD results, the 2- or 6-H can more easily interact with Leu^{17}. [g] 3, 5-H of Phe^{14} and γH of Leu^{17} also show cross-peaks which, having lower intensities, are assigned to secondary NOE. [h] γMe and δMe are overlapped; from MD results, δMe is the group involved in the NOE interaction.

random coil values[18] for the NH and αH protons (Table 1) is very large. An alternating trend of the chemical shift deviations was observed along the whole peptide segment, not only in the α-helix portion: Ser^5, Asp^8, Cys^{11}, His^{16} and Ile^{19} NH protons show more than 0.5 ppm upfield shifts with respect to the random coil values, whereas Cys^{15} and especially Ser^2 and Ser^4 NH display large lowfield shifts (0.55 and 0.77 ppm respectively). The deviation in αH values is a little less

pronounced: all protons, except those of Ser^2 and Cys^3, are shielded, Lys^9, Val^{12} and Phe^{14} showing the largest shift (0.4–0.6 ppm). Only for Glu^{10} and Leu^6, are both the NH and αH deviations within ±0.2 ppm. These data indicate that **ET-1** exhibits an ordered structure in water solution, but any other interpretation of the chemical shift values is difficult and hazardous.

On the other hand, we tried to obtain all possible information from the changes with temperature and pH of the amide chemical shifts and from deuterium exchange experiments. The NH variation with temperature, within the range 5–23 °C, is small (0.15 ppm upfield for Cys^3 and Ile^{20}, 0.05 ppm lowfield only for Asp^8 and Cys^{11}), in agreement with the same NOE results obtained at 5 and 23 °C. The temperature coefficients $\Delta\delta/\Delta T$ also appeared quite constant, in the range −1 to −5 ppb °C^{-1}, except for the terminal Ser^2 (−7.7), Cys^3 (−8.3), Ile^{20} (−8.8) and for Asp^8 (+3.3) and Cys^{11} (+2.2). If we consider, as suggested by Andersen *et al.*[5], the plot of $\Delta\delta/\Delta T$ *versus* the deviations from standard values,[17] $\Delta\delta$rc, a very scattered map results, as expected from an unchanged conformational equilibrium.

The chemical shift variation with pH of amide and αH protons (see Table 1) are not very large, except for Trp^{21} (NH +0.39, αH −0.52 ppm downfield and upfield shift respectively at acidic pH), for Leu^{17} (NH −0.28, αH −0.17 ppm), for Cys^{11} and Val^{12} (NH −0.22 ppm), for Ser^4 (NH −0.24 ppm) and Asp^8 (αH −0.24 ppm).

The exchange experiments of amide protons, performed with D_2O at 5 °C and acidic pH, showed that Ser^2, Ser^4, Cys^3, Asp^{18}, Trp^{21} and Leu^6 (or Cys^{15})* exchange completely within 5 min; Met^7, Asp^8, Glu^{10} and Cys^{15} (or Leu^6)* exchange within 25 min. In contrast, the signals of Lys^9, Cys^{11}, Val^{12}, Phe^{14}, His^{16}, Ile^{19} and Ile^{20} were still visible after 2 h at 5 °C, and those of Phe^{14} and Ile^{20} did not disappear completely after 3 h at 12 °C. Of the remaining three signals at δ 7.78–7.80 (Ser^5, Trp^{13}, Leu^{17}), two exchange rapidly (presumably Ser^5 and Leu^{17}), the other disappears after 2 h at 5 °C; their identification is not straightforward, due to partial signal overlap.

These data are in agreement with the helix conformation suggested by the NOE results, as the slow exchange of 12, 13, 14 and to a lesser extent of 15 amide protons indicates that the helix is stabilized by at least three or four CO_i–NH_{i+4} hydrogen bonds. Distances of *ca.* 2 Å were found, in the structures obtained by MD, between the pairs 9-CO–13-NH, 10-CO–14-NH and 11-CO–15-NH, whereas 12-NH shows distances of *ca.* 2.8 and 2.5 Å from 8-CO and 9-CO respectively. Actually Asp^8 is not in the helix segment, thus the distance for the (i, $i + 4$) hydrogen bond is no longer present, but the slow exchange of 12-NH can be explained with the protection from water by the disulfide bridges. Lys^9 and Cys^{11} amide protons can form hydrogen bonds with the carboxy group of Asp^8, as distances of *ca.* 2 Å were found, in agreement with the deuterium exchange experiment. However the most interesting result was the finding that Ile^{20} and Ile^{19} exchange very slowly, because this suggests the presence of hydrogen bonding which might be responsible for a well defined structure for the C-terminal tail. The 7.0–9.0 Hz values of $J_{\alpha NH}$ for residues 17–21, together with the absence of (i, $i + 3$) NOE interactions, prove the absence of helical structure for this segment. The isolated $d_{\alpha NH}$ (i, $i + 2$) connectivity observed between Ile^{19} and Trp^{21} might be indicative of a turn conformation for the segment 18–21, but the identification of turns are always difficult.

The N-terminal segment shows interesting long-range NOE contacts: Ser^2αH with a methyl group of Leu^6, Leu^6αH with the pro-*S* methyl group of Val^{12}; the same Me group of Val^{12} with the pro-S βH of Cys^3, the pro-*R* βH of Cys^3 with the pro-*R* βH of Cys^{11}, the upfield βH of Ser^5 † with Asp^8NH and with the pro-*R* βH of Cys^{11}. In addition, an isolated (i, $i + 2$) αH–NH NOE interaction between Ser^5 and Met^7, together with strong and isolated (i, $i + 1$) NH–NH and αH–NH interactions between residues 6–7 and 5–6 respectively, suggested a turn secondary structure for the fragment 4–7. An inspection of the distances between C_α atoms, obtained by MD, indicate that a turn-like structure is preferable for the segment 5–8.

Inter-proton Distance Constraints and Structure Derivation of **ET-1** *at Neutral pH.*—The volumes of 170 NOE cross-peaks were integrated and translated into interatomic distances. At the correlation time of 2 ns, the amount of spin diffusion was neglibible and did not lead to serious errors in the determination of the distances. In fact theoretical calculations of 2D-NOESY intensities with a complete relaxation matrix approach showed that the NOE build-up for different model geometries and spin systems is linear up to 400 ms.

170 Interatomic distances, 7 dihedral angles θ and 23 additional constraints with only a lower boundary were used for the simulated annealing procedure. These latter constraints correspond to distances ≥5 Å, *i.e.* between protons not involved in NOE interactions. The θ angles, defining the rotation around the N–C_α bond in the fragments H–N–C_α–H were obtained[18] from $J_{\alpha.NH}$ values (Table 2) and were set with an interval of ±10°. The seven residues for which the dihedral angle θ was taken into account as a constraint were Ser^2, Cys^3, Leu^6, Met^7, Ile^{19}, Ile^{20} and Trp^{21}, because the high value of the coupling constants $J_{\alpha,NH}$ is clear evidence of a *trans* orientation of αH and NH protons. The appropriate sign of θ angles was chosen after observing the values of the relative residues in the structures derived from the first calculation, in which these constraints were not applied. The upper and lower bounds for the distance constraints were chosen by adding ±0.3 Å to the values obtained from NOE experiments. When the integrated volume of the NOE cross-peak was very low, for instance in the case of some long-range interactions, an interval of ±0.6 Å was used. A pseudoatom was employed whenever a stereospecific assignment of the proton could not be performed or when a proton of a methyl group was involved. In these cases an additional 0.8–1.0 Å was added to the upper bound distance. The stereospecific assignment of the protons involved in the NOE interactions, *i.e.* βH in residues 3, 7, 8, 9, 11, and Me groups in Val^{12} was accounted for in the MD simulation.

Of the 200 structures derived from the above described procedure, 40 were found to satisfy the NOE constraints within 0.5 Å, but they were clustered in two different families. Upon careful analysis it was found that one of the two sets of structures gave rise to proton interactions which were not observed in the spectra. These structures (22 in number) were therefore eliminated and the constraint file was modified accordingly to avoid recurrence of the unwanted interactions. As the single protons of the aromatic ring in Tyr^{13} and Phe^{14} residue could not be distinguished, due to the symmetry of the ring, in the first calculation a pseudoatom in the centre of the aromatic rings was used along with a higher upper bound distance constraint. Because of this fact, it was observed that in the 18 remaining structures the position of the side chains of residues 13 and 14 was not very uniform. It was also observed, however, that the protons involved in NOE interactions with the side chains of Tyr^{13} and Phe^{14} were clearly positioned at the opposite sides of the residues themselves. As a consequence

* Leu^6 and Cys^{15} NH signals are very close and often overlap.

† The stereospecific assignment of Ser^5 β-protons, although nonequivalent, is uncertain.

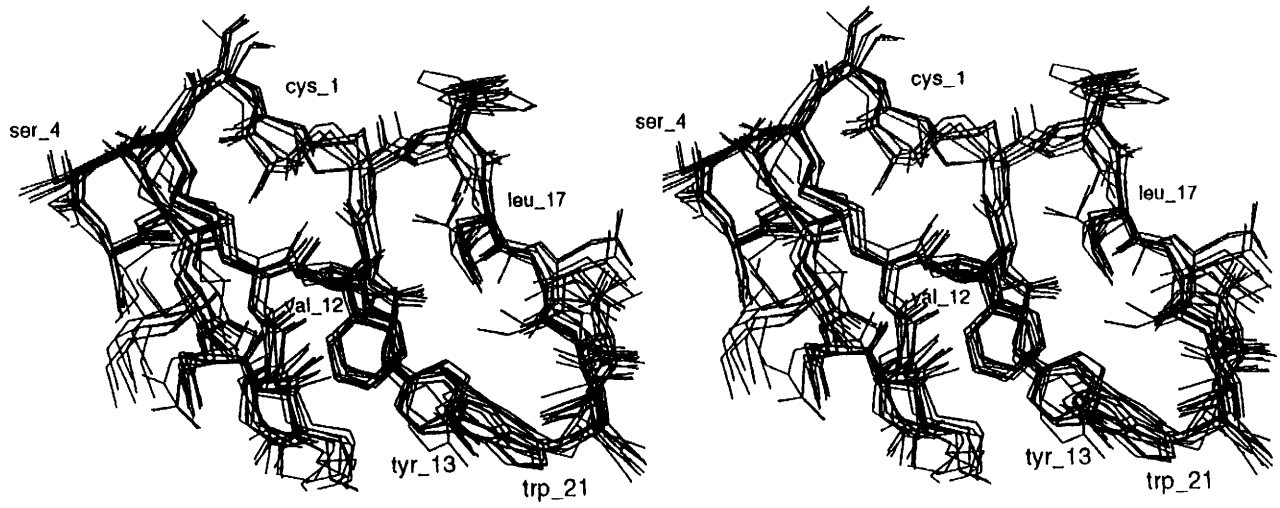

Fig. 3 Stereoview of the eleven structures that best fitted the experimental NOE data, obtained in water at neutral pH

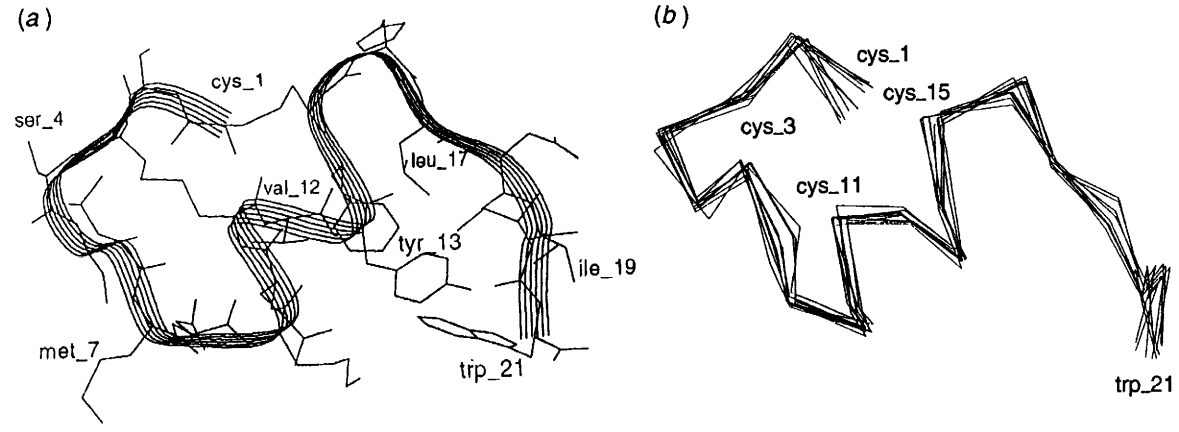

Fig. 4 (*a*) One of the 11 best structures; (*b*) view of the backbones (C_α atoms only) for the family of the best 11 structures

we reasoned that the NOE interactions would involve protons at the opposite sides of the aromatic rings. Therefore we decided to remove the pseudo atoms at the centre of the rings and substitute them with specific assignments of the aromatic protons of the residues.

With these minor modifications a further constrained MD at 300 K for 10 ps was performed, followed by a constrained minimization. This yielded 11 structures which satisfied all the interproton distances within 0.3 Å. In addition, the positioning of the side chains of residues 13 and 14 was more uniform, as can be seen from Fig. 3, where the 11 structures are represented superimposed. Fig. 4 shows one of these structures and a view of the backbone C_α atoms for this family of **ET-1** structures. It can be seen that the NOE data tightly define the whole backbone conformation: the segment 9–16 forms a right-handed α-helix, with a slight deformation at the level of Cys^{15}; the two terminals form loops, similar to turn structures, which are folded back toward the core of the helix. The helix deformation at Cys^{15} is better shown in the diagram of φ and ψ angles (Fig. 5), where small deviations appear at the level of residues 15–17, *i.e.* at the end of the helix. The end of the helix is also shown by the absence of the characteristic CO_i–NH_{i+4} hydrogen bonds between His^{16}NH and the carbonyl oxygen of Val^{12} and by irregular distances between 15-NH and 11-CO. These results are in agreement with the values of $J_{\alpha,NH}$ (Table 2) and with the deuterium exchange experiments described before. The N-terminal segment appears quite accessible to water, the NH protons exhibiting in general very fast exchange, whereas the α-helix core and the C-terminal represent the hydrophobic part of the molecule. All the NHs of this part exchange slowly, except for 21, 18 and 17 residues.

The conformation of both N- and C-terminals are also well defined, as appears clearly from the good superposition of the values of φ and ψ angles, reported in Fig. 5, for the best eleven structures. The side-chains also display ordered structures, adopting compact conformations, with the indole ring of Trp^{21} in close proximity to the pro-*R* methyl groups of Val^{12} and to the atoms of Lys^{9}. This leads to some packing of the aromatic rings of Tyr^{13}, Phe^{14} and Trp^{21}, thus allowing hydrophobic interactions, which should stabilize the folded conformations. This is very likely, as in such a way the hydrophobic residues are protected from the polar medium. This finding is in agreement with the NOE interactions detected between the aromatic protons of Tyr^{13} and Phe^{14}; interactions, which were intentionally not used as constraints in the MD simulation, in order to leave the system free to adapt these hindering groups.

The side-chains of Leu^{17} and Ile^{18} are also close to the aromatic rings of Tyr^{13} and Phe^{14}, which can thus protect from the polar solvent the alkyl groups of the 17 and 19 side-chains. Independent evidence of the poor accessibility of the water solvent in this region comes from the very slow deuterium exchange of the NH proton of both Ile^{19} and Ile^{20}. In addition Ile^{19} NH can form a hydrogen bond with the side-chain carboxy group of Asp^{18}. This might be reflected in some change with pH of the 19-NH chemical shift, which actually does not occur. The shift variation with pH, as stated above, concerns the residues 4, 11, 12, 17 and 21. In our model, the NH of Cys^{11} can form a hydrogen bond with a carboxy group, specifically that of Asp^{8} (2.01 Å), whereas all the others apparently cannot. The NH proton of Leu^{17}, instead, is able to interact with one nitrogen atom of the Hys^{16} aromatic ring and Ser^{4}NH with the

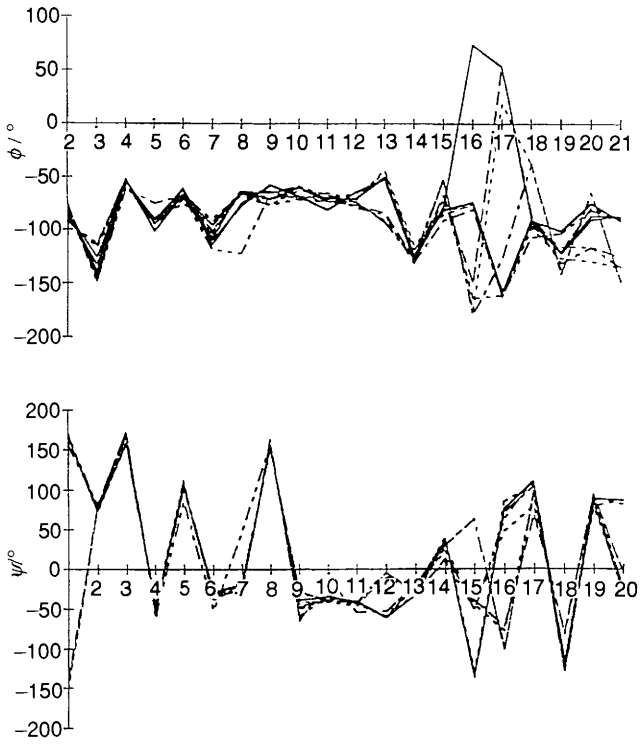

Fig. 5 Summary of Φ and ψ angles for the best 11 structures. The angles are defined following the standard nomenclature (IUPAC–IUB), *i.e.* Φ_i CO_{i-1}–N_i–αC_i–CO_i, ψ_i N_i–αC_i–CO_i–N_{i+1}. The residue numbers are given on abscissa.

sulfur atom of Cys^3. However the interpretation of chemical shift is always difficult and small variation with pH, as those observed (0.2–0.3 ppm) might be insignificant. In addition the MD simulation did not take into account solvent water molecules, which are known to be very important for the occurrence of electrostatic interactions, including hydrogen bonding.

We can note that the last residue, Trp^{21}, shows the largest variation with pH, involving also αH (0.5 ppm); in addition, we observed some slight differences in the NOE interactions at acidic pH compared to the situation at neutral pH, *i.e.* Lys^9 no longer shows contacts with the indole ring, as already mentioned. The two effects might be connected and they can be explained with slight conformational changes, induced by the protonation of the Lys^9 NH_2 group. Actually Lys^9 does not show other long-range interactions and it is likely that the positively charged amino group, which at neutral pH can interact with the ionized carboxy group of either Glu^{10} or Asp^8, is now projected toward the polar solvent. It is not so unusual that in proteins the net charge can be varied over wide limits without any significant change in structure, even in cases where dramatic effects of charge variation on biological activity was observed.[21] In **ET-1** molecule, Lys^9 is probably located in a secondary site, since the functional activity appeared unaffected by a leucine replacement at 9-position.[16]

Conclusions

The present study has shown that **ET-1** in water displays a highly ordered tertiary structure, adopting compact conformations, with the indole ring of Trp^{21} folded back toward the α-helical segment (9–16 residue), in close proximity to the pro-*R* methyl group of Val^{12}. The C-terminal tail, determinant for the binding with the receptor and for its activation, is also well defined by many long-range NOE interactions between the tail and the core of the molecule. The family of eleven structures, which satisfy[5] the experimental data to within 0.3 Å, has indicated that the C-terminal adopts a definite preferred conformation. This conclusion is important for two reasons: (*i*) it is the first structure determination of **ET-1** in native solvent and correlations with binding studies can thus be performed with more confidence; (*ii*) in all the previous investigations on **ET-1**, except for one study in Me_2SO,[2a] the C-terminal remained undefined. The results in Me_2SO[2–4] were quite divergent. A helical segment was always detected, whereas only in the paper of Saudek *et al.*[2a] the C-terminal was suggested to be folded toward the bicyclic part of **ET-1**. On the other hand, Andersen *et al.*[5] reached the conclusion that 'motional averaging in Me_2SO is so extensive as to preclude structure definition by the NOE method'.

Studies on endothelin-3 in acetic acid–H_2O solvent[2b] and in water with *ca.* an equimolar concentration of sodium azide[9] have shown that the C-terminal folds back towards the opposite face of the helix.

From our results, we can also conclude that the compact conformation of **ET-1** is rather stable, even at room temperature, at neutral and acidic pH. Hydrophobic interactions involving the aromatic rings of Tyr^{13}, Phe^{14} and Trp^{21} concur in stabilizing the folded conformations, thus creating a small cavity which also contains the alkyl groups of 17, 19 and 20 side-chains. In such a way, they become protected from the polar solvent, as indicated by the slow exchange with D_2O of the amidic protons of isoleucine 19 and 20, which proves the poor accessibility of water in this region.

Acknowledgements

This work was supported by the National Research Council (C.N.R.), *Progetto Finalizzato Chimica Fine II.*

References

1 M. Yanagisawa, H. Kurihara, S. Kimura, Y. Tomobe, M. Kobayashi, Y. Mitsui, Y. Yazaki, K. Goto and T. Masaki, *Nature*, 1988, **332**, 411.
2 (*a*) V. Saudek, J. Hoflack and J. T. Pelton, *Int. J. Peptide Protein Res.*, 1991, **37**, 174; (*b*) P. Bortmann, J. Hoflack, J. T. Pelton and V. Saudek, *Neurochem. Int.*, 1991, **18**, 491, and refs. therein.
3 S. Endo, H. Inooka, Y. Ishibashi, C. Kitada, E. Mizuta and M. Fujino, *FEBS Lett.*, 1989, **257**, 149.
4 S. Munro, D. Craik, C. McConville, J. Hall, M. Searle, W. Bicknell, D. Scanlon and C. Chandler, *FEBS Lett.*, 1989, **278**, 9.
5 N. H. Andersen, C. Chen, T. M. Marschner, S. R. Krystek Jr. and D. A. Bassolino, *Biochemistry*, 1992, **31**, 1280.
6 M. D. Reily and J. B. Dumbar Jr., *Biochem. Biophys. Res. Commun.*, 1991, **178**, 570.
7 D. C. Dalgarno, L. Slater, S. Chackalamannil and M. M. Senior, *Int. J. Pept. Protein Res.*, 1992, **40**, 515.
8 A. Aumelas, L. Chiche, E. Mahe, D. Le-Nguyen, P. Sizun, P. Berthault and B. Perly, *Int. J. Pept. Protein Res.*, 1991, **37**, 315.
9 R. G. Mills, S. I. O'Donoghue, R. Smith and G. F. King, *Biochemistry*, 1992, **31**, 5640.
10 R. Bennes, B. Calas, P.-E. Chabrier, J. Demaille and F. Heitz, *FEBS Lett.*, 1990, **276**, 21.
11 J. Vane, *Nature*, 1990, **348**, 673; J. R. Vane, E. E. Änggard and R. M. Botting, *New England J. Med.*, 1990, **323**, 27; H. Arari, S. Hori, I. Aramori, H. Ohkubo and S. Nakanishi, *Nature*, 1990, **348**, 730; T. Sakurai, M. Yanagisawa, Y. Takuwa, H. Miyazaki, S. Kimura, K. Goto and T. Masaki, *Nature*, 1990, **348**, 732; for a perspective review see A. M. Doherty, *J. Med. Chem.*, 1992, **35**, 1493.
12 T. Masaki and M. Yanagisawa, *Med. Res. Rev.*, 1992, **12**, 391.
13 J. H. B. Pease and D. E. Wemmer, *Biochemistry*, 1988, **27**, 8491.
14 C. Takasaki, M. Yanagisawa, S. Kimura, K. Goto and T. Masaki, *Nature*, 1988, **335**, 303.
15 M. Clozel, V. Breu, K. Burri, J.-M. Cassal, W. Fischli, G. A. Gray, G. Hirth, B.-M. Löffler, M. Müller, W. Neidhart and H. Ramuz, *Nature*, 1993, **365**, 759.
16 J. T. Hunt, V. G. Lee, P. D. Stein, A. Hedberg, E. C.-K. Liu, D. McMullen and S. Moreland, *Biorg. Med. Chem. Lett.*, 1991, **1**, 33, and references quoted therein.

17 P. J. Hore, *J. Magn. Reson.*, 1983, **55**, 283.
18 K. Wüthrich, *NMR of Proteins and Nucleic Acids*, Wiley, New York, 1986
19 C. R. Cantor and P. R. Schimmel, *Biophysical Chemistry, Part II*, W. H. Freeman and Co., New York, 1980, p. 461.
20 S. Hyberts, W. Mäkri, G. Wagner, *Eur. J. Biochem.*, 1987, **164**, 625; G. Wagner, M. Vasak, J. H. R. Kägi and K. Wüthrich, *J. Mol. Biol.*, 1988, **201**, 637.
21 T. E. Creighton, *Protein Folding*, W. H. Freeman and Co., New York, 1992, p. 37.

Paper 3/07266E
Received 8*th December* 1993
Accepted 28*th January* 1994